

Figure 1: An example of the instantaneous profit maximisation algorithm. The carbon gain (green), hydraulic cost (purple), and net profit (blue) are shown as functions of the transpiration stream, which ranges between the soil water potential at saturation (Ψ_{sat}) and the critical water potential (Ψ_{crit}). Maximum hydraulic conductance (k_{\max}) was calculated for each of the three behavioural solutions (i.e. $k_{\max,\text{high}}$, $k_{\max,\text{opt}}$, and $k_{\max,\text{low}}$; cf. Section 2 of the Materials and Methods), before being used as an input the model. The dashed and dotted lines illustrate the impacts of alternative strategies for k_{\max} on the maximum profit; the optimal leaf water potentials ($\Psi_{\text{leaf},\text{opt}}$) at which profit is maximised span a range of 0.4 MPa between the instantaneous model run using $k_{\max,\text{high}}$ and the one using $k_{\max,\text{low}}$. The species used in this example is *Juniperus virginiana* ($P_{50}=-6.6 \text{ MPa}$ and $P_{88}=-10.5 \text{ MPa}$; Choat et al., 2012), with $V_{\text{cmax},25}=100 \mu\text{mol m}^{-2} \text{s}^{-1}$, $T_{\text{air}}=25^\circ\text{C}$ and $D=1 \text{ kPa}$, $\Psi_s=-0.8 \text{ kPa}$, and $\text{LAI}=2 \text{ m}^2 \text{ m}^{-2}$.

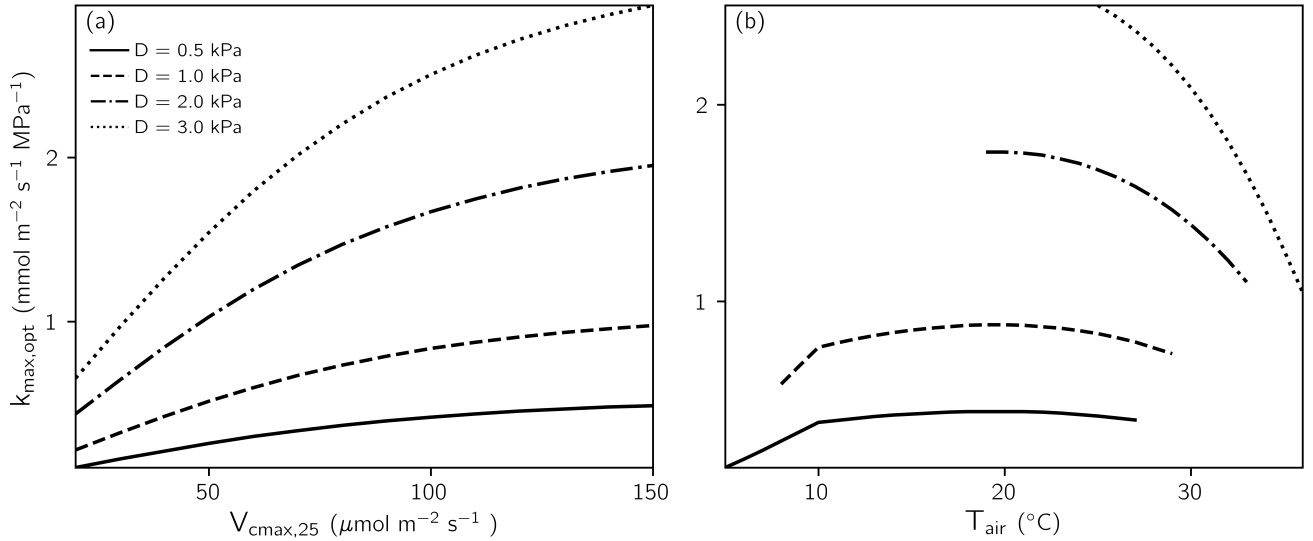


Figure 2: The sensitivity of the modelled optimal coordination between the maximum hydraulic conductance ($k_{\text{max},\text{opt}}$) and (a) the maximum carboxylation rate at 25°C ($V_{\text{cmax},25}$) and (b) air temperature (T_{air}), both depending on vapour pressure deficit (D). In panel a, $k_{\text{max},\text{opt}}$ increases near proportionally with $V_{\text{cmax},25}$ and in a logarithmic fashion with D; T_{air} is fixed to 25 °C. In panel b, $k_{\text{max},\text{opt}}$ increases with T_{air} , before decreasing (sharply at the two highest D) starting between 20 – 25 °C; $V_{\text{cmax},25}$ is set to 100 $\mu\text{mol m}^{-2} \text{s}^{-1}$. The valid range for $k_{\text{max},\text{opt}}$ is constrained by physically plausible co-occurring values of T_{air} and D under a relative humidity spanning 5 – 95%. The species used in this example is *Juniperus virginiana* (P50=−6.6 MPa and P88=−10.5 MPa; Choat et al., 2012), with Ψ_s =−0.8 kPa, and LAI=2 $\text{m}^2 \text{m}^{-2}$.

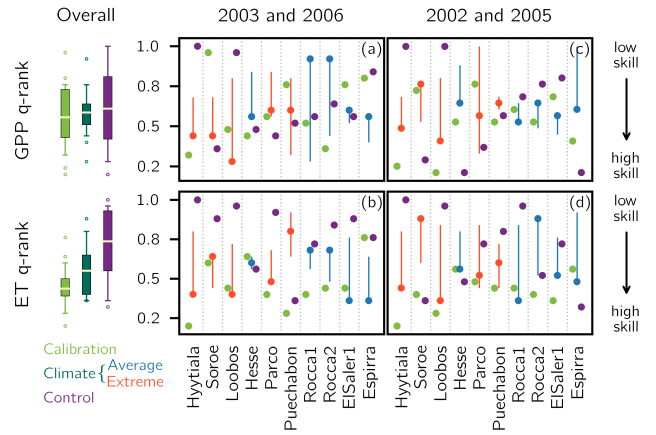


Figure 3: Quantile ranks of the best configurations of the Profitmax model compared to the Control model, across drought (panels a and b) and non-drought years (panels c and d), and for Gross Primary Productivity (GPP; panels a and c) and Evapotranspiration (ET; panels b and d). The vertical lines – blue (Average scenario) or red (Extreme scenario) – correspond to the best climate configuration range of ranks across the three behavioural solutions for the maximum hydraulic conductance. The box and whisker plots to the right of the figure show summaries of the ranks across sites, but do not account for the behavioural range shown by the vertical lines. In the box and whiskers plots, the horizontal yellow line shows the average overall quantile rank, and the box shows the interquartile range; the whiskers extend to the 10th and 90th percentile values of the ranks, with dots outside of the whiskers showing outliers.

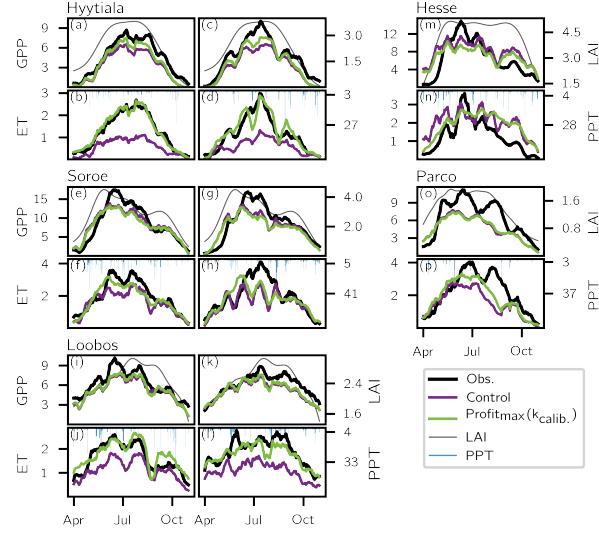


Figure 4: A 14-day running average of the carbon and water fluxes predicted by the best selected calibration configuration from the Profitmax model (green line) at the five northernmost eddy-covariance sites during the 2003 (panels a, b, e, f, i, j, m, n, o, p) and 2006 (panels c, d, g, h, k, l) European drought events, compared to the Control model (purple line), and to the observations (black line). Grey lines show the prescribed phenologies (LAI, $m^2 m^{-2}$) and blue bars the daily precipitation (PPT, mm d $^{-1}$). The Gross Primary Productivity (GPP) is in g C m $^{-2}$ d $^{-1}$ and the Evapotranspiration (ET) in mm d $^{-1}$.

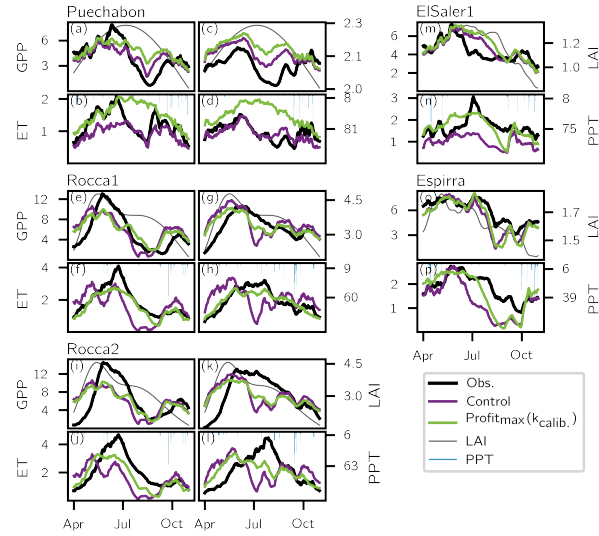


Figure 5: A 14-day running average of the carbon and water fluxes predicted by the best selected calibration configuration from the Profitmax model (green line) at the five southernmost eddy-covariance sites during the 2003 (panels a, b, e, f, i, j, m, n, o, p) and 2006 (panels c, d, g, h, k, l) European drought events, compared to the Control model (purple line), and to the observations (black line). Grey lines show the prescribed phenologies (LAI, $m^2 m^{-2}$) and blue bars the daily precipitation (PPT, mm d $^{-1}$). The Gross Primary Productivity (GPP) is in g C m $^{-2}$ d $^{-1}$ and the Evapotranspiration (ET) in mm d $^{-1}$.

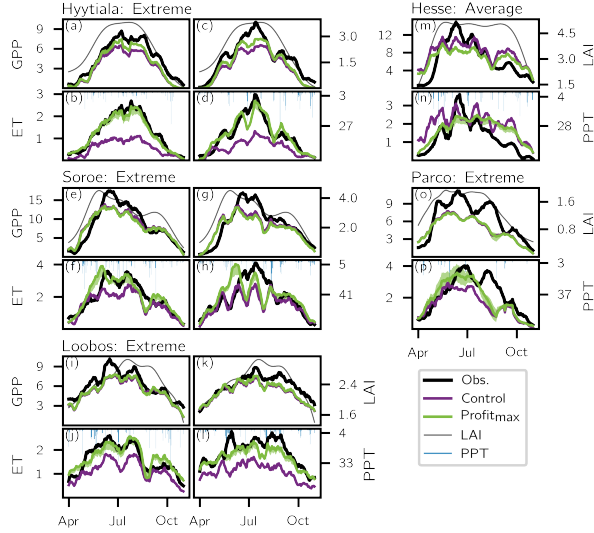


Figure 6: A 14-day running average of the carbon and water fluxes predicted by the best selected calibration configuration from the Profitmax model (green line) at the five northernmost eddy-covariance sites during the 2003 (panels a, b, e, f, i, j, m, n, o, p) and 2006 (panels c, d, g, h, k, l) European drought events, compared to the Control model (purple line), and to the observations (black line). The green line is the kmax,opt strategy and the green shadings encompass the instantaneous range of fluxes predicted by the three behavioural solutions for kmax. Grey lines show the prescribed phenologies (LAI, $m^2 m^{-2}$) and blue bars the daily precipitation (PPT, mm d $^{-1}$). The Gross Primary Productivity (GPP) is in g C m $^{-2}$ d $^{-1}$ and the Evapotranspiration (ET) in mm d $^{-1}$.

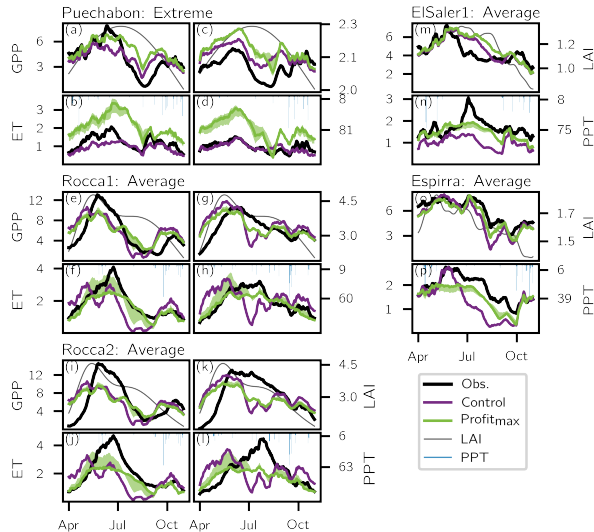


Figure 7: A 14-day running average of the carbon and water fluxes predicted by the best selected calibration configuration from the Profitmax model (green line) at the five southernmost eddy-covariance sites during the 2003 (panels a, b, e, f, i, j, m, n, o, p) and 2006 (panels c, d, g, h, k, l) European drought events, compared to the Control model (purple line), and to the observations (black line). The green line is the kmax,opt strategy and the green shadings encompass the instantaneous range of fluxes predicted by the three behavioural solutions for kmax. Grey lines show the prescribed phenologies (LAI, $m^2 m^{-2}$) and blue bars the daily precipitation (PPT, mm d $^{-1}$). The Gross Primary Productivity (GPP) is in g C m $^{-2}$ d $^{-1}$ and the Evapotranspiration (ET) in mm d $^{-1}$.

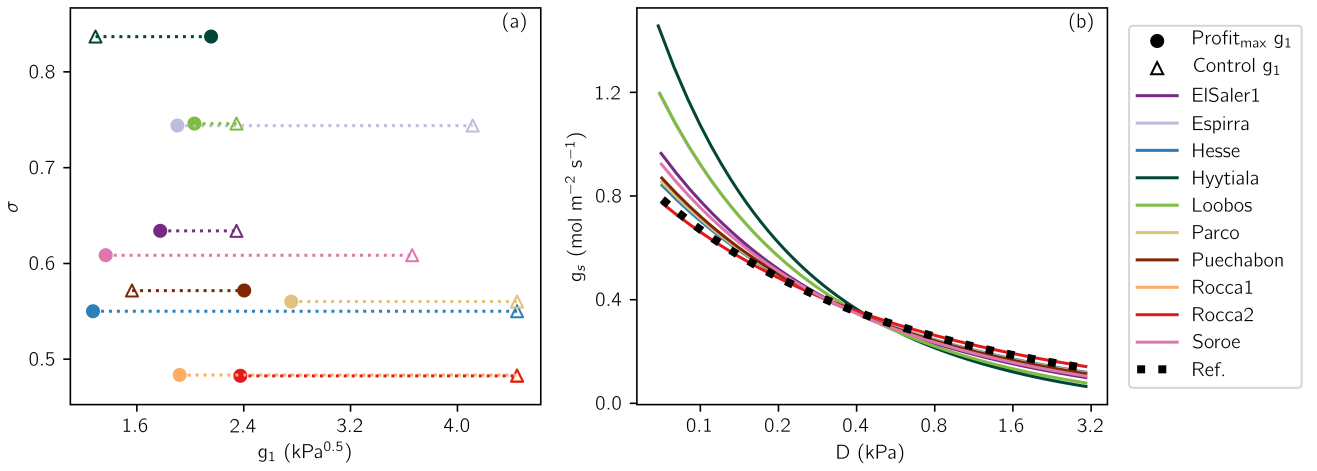


Figure 8: A comparison of the sensitivity of the Control and calibrated Profitmax models' stomatal conductance (g_s) to vapour pressure deficit (D) across the 10 eddy-covariance sites. Panel (a) shows the relationship between the implied water use efficiency (g_1 , $\text{kPa}^{0.5}$) of the calibrated Profitmax model and its sensitivity to D (σ , unitless). The values of g_1 obtained for the Profitmax model were converted from unit $\text{kPa}\sigma$ to unit $\text{kPa}^{0.5}$ for comparison with the values of g_1 used in the Control model. g_1 and σ were obtained by least-square fitting of the g_s simulated by the calibrated Profitmax model to the Medlyn et al. (2011) stomatal conductance model. The estimates were produced using the site hydraulic and photosynthetic parameters, for temperatures ranging $10 - 40^\circ\text{C}$ and D ranging $0.05 - 3$ kPa . The values of g_1 used in the Control model are plotted against the respective sites' σ for visual comparison with those of the Profitmax model only, as they correspond to $\sigma = 0.5$. Panel (b) shows the effect of the various σ on the g_s given by the Control model at 25°C . The input parameter g_1 was set to $2 \text{ kPa}^{0.5}$ for all the generated curves, but it was transformed to $\text{kPa}\sigma$ upon running the Control model with the site-specific values of σ shown in panel a. The reference g_s of the Control model ($\sigma = 0.5$) is plotted for comparison. For both panels a and b, the models were run assuming well-watered conditions.

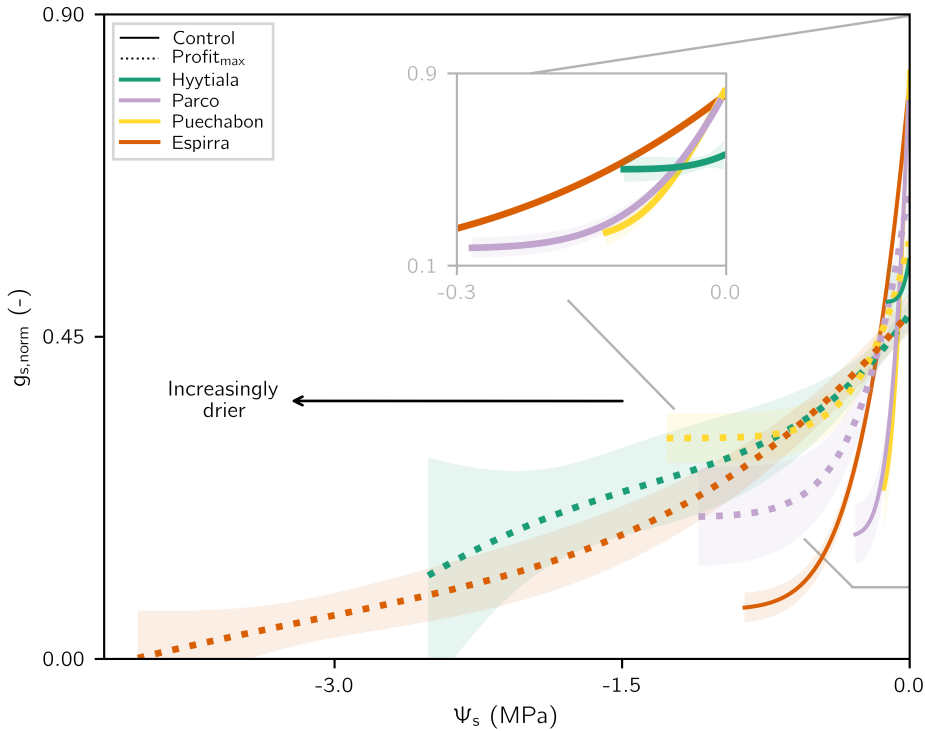


Figure 9: A comparison of the decline in stomatal conductance (g_s) with predawn soil water potential (Ψ_s), for the Control (plain lines) and the calibrated Profitmax (dotted lines) models at a sub-selection of sites. The functional forms emerge from the soil parameters and the β functions in the Control, and from the plant hydraulic traits and the profit maximisation algorithm in the best selected calibration. The inset zooms on the functional forms of the $g_s - \Psi_s$ curves from the Control model for $\Psi_s > -0.3$ MPa. The functional forms are made comparable by normalising g_s by its maximum at a given site. Note that seemingly slow decreases in g_s with Ψ_s can be attributed to the non-linear relationship between Ψ_s and volumetric soil moisture, whereby small variations in the latter can lead to large variations in the former. To avoid rainfall effects, the data up to 48 hours after rain were excluded. To avoid low solar radiation and low temperature effects, the g_s data were restricted between 9:00 h – 15:00 h from April – November across all years. The curves were fitted with a linear generalised additive model and the shadings show the 95% confidence interval of the fit.

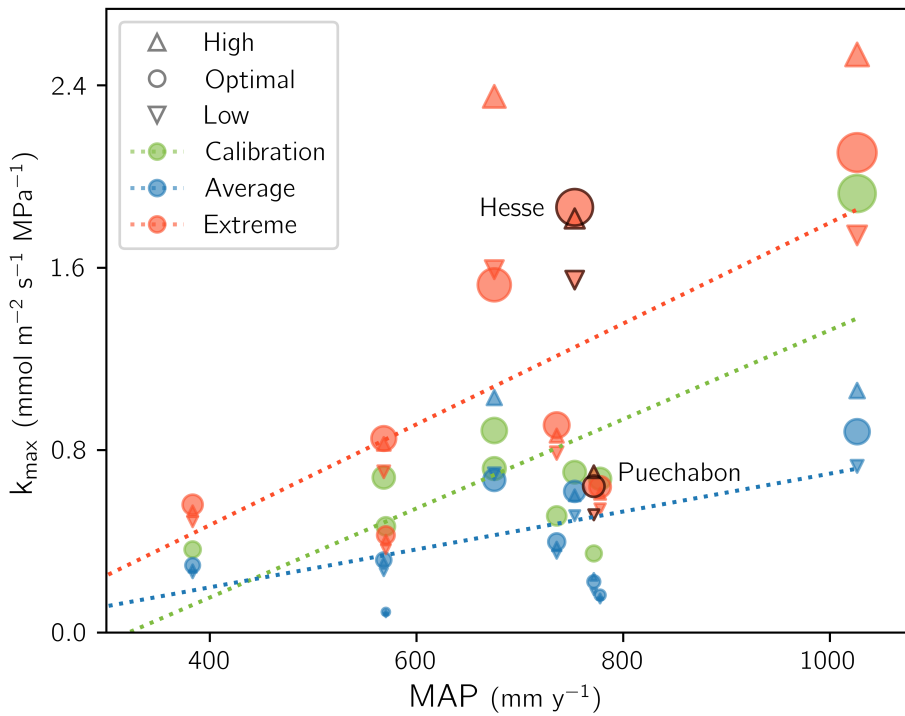


Figure 10: The estimated site maximum hydraulic conductance (k_{\max}), for each climate configuration of the Profitmax model and for the best selected calibration, shown as a function of Mean Annual Precipitation (MAP; as listed in Table 2). Note, the MAP was not used in the estimation of k_{\max} , however k_{\max} was multiplied by the sites' weighted composite LAI, which normalises it to ground area and makes it comparable across sites. Linear regressions are used to show the positive relationship between k_{\max} and MAP, with a r^2 of 0.53 and a p-value of 0.02 for the best selected calibration, a r^2 of 0.21 and a p-value of 0.01 for the Average climate scenario, and a r^2 of 0.30 and a p-value of 0.002 for the Extreme climate scenario.